

# Pneumatic Energy Sources for Autonomous and Wearable Soft Robotics

Michael Wehner,<sup>1,2</sup> Michael T. Tolley,<sup>1,2</sup> Yiğit Mengüç,<sup>3</sup> Yong-Lae Park,<sup>4</sup> Annan Mozeika,<sup>5</sup> Ye Ding,<sup>1</sup> Cagdas Onal,<sup>6</sup> Robert F. Shepherd,<sup>7</sup> George M. Whitesides,<sup>2,8</sup> and Robert J. Wood<sup>1,2</sup>

## Abstract

Many pneumatic energy sources are available for use in autonomous and wearable soft robotics, but it is often not obvious which options are most desirable or even how to compare them. To address this, we compare pneumatic energy sources and review their relative merits. We evaluate commercially available battery-based microcompressors (singly, in parallel, and in series) and cylinders of high-pressure fluid (air and carbon dioxide). We identify energy density (joules/gram) and flow capacity (liters/gram) normalized by the mass of the entire fuel system (versus net fuel mass) as key metrics for soft robotic power systems. We also review research projects using combustion (methane and butane) and monopropellant decomposition (hydrogen peroxide), citing theoretical and experimental values. Comparison factors including heat, effective energy density, and working pressure/flow rate are covered. We conclude by comparing the key metrics behind each technology. Battery-powered microcompressors provide relatively high capacity, but maximum pressure and flow rates are low. Cylinders of compressed fluid provide high pressures and flow rates, but their limited capacity leads to short operating times. While methane and butane possess the highest net fuel energy densities, they typically react at speeds and pressures too high for many soft robots and require extensive system-level development. Hydrogen peroxide decomposition requires not only few additional parts (no pump or ignition system) but also considerable system-level development. We anticipate that this study will provide a framework for configuring fuel systems in soft robotics.

## Introduction

THE FIELDS OF MOBILE and wearable soft robotics are rapidly evolving, using flexible low-modulus materials often inspired by structures found in nature.<sup>1–5</sup> As complementary technologies to traditional robotics, mobile and wearable soft robotics are well suited for human-safe environments and a compelling option for industrial, home, rehabilitation, and surgical applications.<sup>6–9</sup> Soft robots can take many forms (Fig. 1) and can be designed to perform a variety of locomotion and manipulation tasks,<sup>10,11</sup> such as walking,<sup>1</sup> rolling,<sup>12</sup> grasping,<sup>13,14</sup> swimming,<sup>15</sup> and jumping.<sup>6</sup> Soft wear-

able robotics can be used for augmentation,<sup>16</sup> rehabilitation,<sup>17</sup> injury prevention,<sup>18–20</sup> and orthotic applications.<sup>2</sup>

Even as the use of pneumatics in soft mobile robotics grows, the most common energy source remains a tether to a stationary compressor. While appropriate for many stationary systems such as surgical robots or some therapeutic applications, a tether is usually undesirable in mobile robotics. This motivates us to explore the characteristic properties of pneumatic energy sources and scaling laws for their use in mobile applications. If one simply selects the technology with the highest energy density, then scale, pressure, and flow rate may be incompatible with system requirements. While no specific

---

<sup>1</sup>School of Engineering and Applied Sciences, Harvard University, Cambridge, Massachusetts.

<sup>2</sup>Wyss Institute for Biologically Inspired Engineering, Harvard University, Boston, Massachusetts.

<sup>3</sup>School of Mechanical, Industrial, and Manufacturing Engineering, Oregon State University, Corvallis, Oregon.

<sup>4</sup>The Robotics Institute, School of Computer Science, Carnegie Mellon University, Pittsburgh, Pennsylvania.

<sup>5</sup>iRobot G and I Research, Bedford, Massachusetts.

<sup>6</sup>Worcester Polytechnic Institute, Worcester, Massachusetts.

<sup>7</sup>School of Mechanical and Aerospace Engineering, Cornell University, Ithaca, New York.

<sup>8</sup>Department of Chemistry and Chemical Biology, Harvard University, Cambridge, Massachusetts.

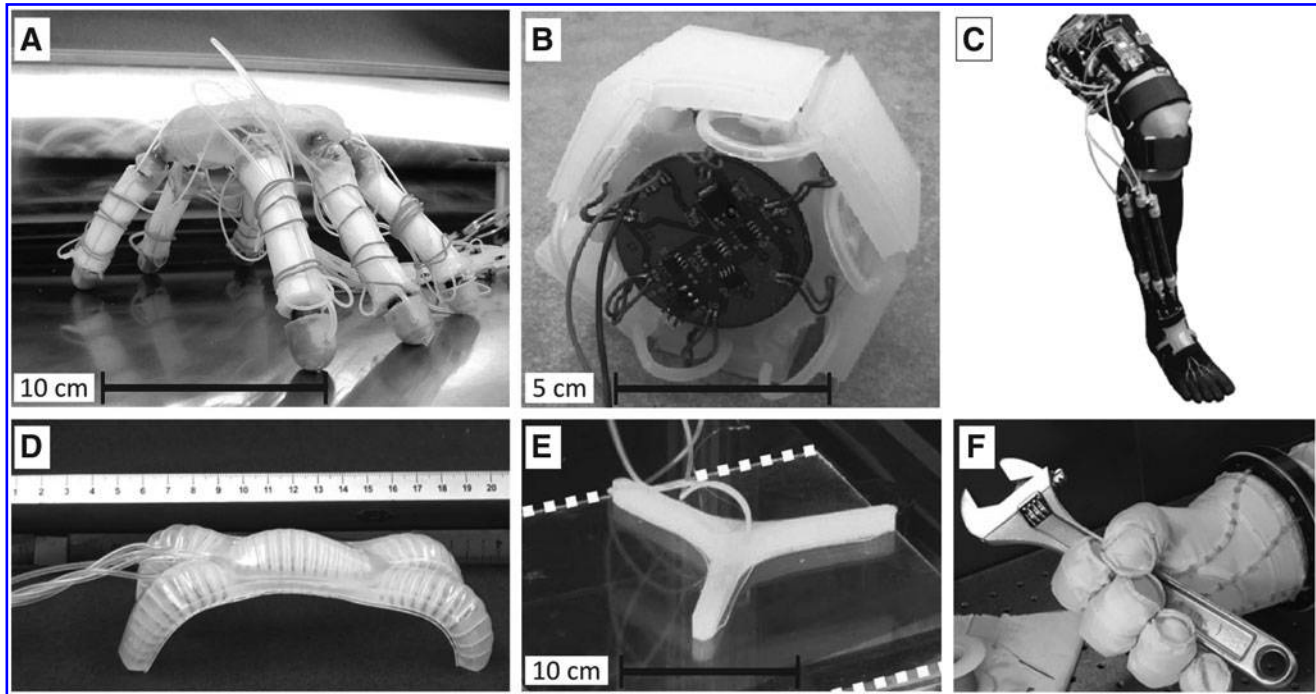


**FIG. 1.** Current soft robots and soft wearable robots. (A) Tethered hexapod (iRobot).<sup>13</sup> (B) Monopropellant-powered soft mobile robot (MIT).<sup>12</sup> (C) Active soft orthotic (Harvard).<sup>2</sup> (D) Soft robot based on PneuNet actuators (Harvard).<sup>1</sup> (E) Explosive jumper methane based (Harvard).<sup>6</sup> (F) Soft hand gripper (iRobot).<sup>13</sup>

size limit bounds this discussion, we focus on devices in the range of tens of grams to a few kilograms with operating pressures in the area of 50–500 kPa (7–74 psi), except as noted. These values are in line with current soft robots<sup>1,7,12</sup> and with artificial muscle (McKibben) actuators often used in wearable robots.<sup>2,5,21</sup> Readers who are unfamiliar with the theory, notation, and principles of pneumatics are urged to review the many resources available on the subject.<sup>22,23</sup>

Pneumatic energy can be stored and released by a variety of means. Air, compressed by a large stationary pump, can be stored in a high-pressure cylinder for later use. Likewise, carbon dioxide (CO<sub>2</sub>) can be stored as a liquid at high pressure and later used as a gas at reduced pressure. Fuels such as methane or butane can be combusted with oxygen at the point of use to quickly release energy in the form of hot high-pressure gas. Monopropellant can be decomposed in the presence of a catalyst to release pressurized gas and heat. Alternately, batteries can power a robot through small, onboard, motorized pumps that pressurize ambient air on demand. In all of these cases, energy is converted into work when pressurized gas expands causing actuation. These technologies utilize direct pressurized gas as well as heat (internally from chemical reaction and absorbed from the environment in polytropic or isothermal expansion) to perform useful work when the gas expands causing actuation. This conversion occurs whether the gas pressure is stored long-term (e.g., in a cylinder) or generated only moments before (e.g., in a pump or by a chemical reaction), making the working fluid the energy storage mechanism as well. Other common transmission systems (hydraulics, gears, cables, and linkages) store little energy in their components, making them fundamentally different from pneumatics; thus, we focus only on the latter here.

We begin with commercially available battery-powered onboard pumps, and cylinders of compressed CO<sub>2</sub> and air. We then discuss direct chemical reaction options (methane and butane combustion and hydrogen peroxide decomposition), which are unavailable as commercial pneumatic systems. For each energy source, we begin with a theoretical description, followed by experimental characterization (where applicable), and conclude with a table of key properties. In describing each technology, some terms are used for consistent comparison:

*Soft robot:* A robot composed entirely or primarily of low-modulus or flexible-inextensible materials. Low-modulus materials are  $\sim 10$  MPa or lower and usually elastomeric (tens to hundreds of percent elastic strain prior to failure, such as silicone and rubber). Flexible-inextensible materials are orders of magnitude stiffer in tension than in bending or shear, such as rope or fabric. Inflatable systems, made of flexible-inextensible materials inflated to a set pressure to maintain their desired form, fall into this category.

*Soft wearable robot:* A device designed to provide sensing or actuation for a wearer. Generally, the wearer’s musculo-skeletal structure provides overall shape, as seen in some orthotics and exoskeletons.

*Net fuel mass:* The mass of actual fuel (compressed air, carbon dioxide, monopropellant, methane, or butane), which scales with system energy capacity.

*Gross fuel mass:* The mass of packaged fuel (battery, cylinder of compressed fluid, or vessel of chemical fuel), which loosely scales with system energy capacity.

*Static mass:* The mass of components required for fuel use (including microcompressors and regulators), which does not

necessarily vary based on fuel tank or battery size, and does not scale with system energy capacity.

*Fuel system mass:* Gross fuel mass plus static mass, which is the total mass of the system required to supply pneumatic energy to the device. This mass does not include components (controller, valve manifold) to distribute fuel within the system in order to provide a consistent comparison between technologies.

*Energy density (net, gross, system):* Energy per mass (J/kg) based on net fuel, gross fuel, or fuel system mass.

*Standard liter:* The volume of a gas normalized to 1 atmosphere absolute (101.3 kPa) and 0°C (STP). This metric is used to calculate flow rates in standard liters per minute (SLM) and total flow.

*Flow capacity:* The total flow available from a source, in standard liters. This can be normalized to standard liters per gram for net, gross, and fuel system capacity.

*Efficiency:* The amount of useable energy under given conditions divided by the total amount of energy in that energy source.

**Microcompressors**

First, we consider compression of ambient air using small onboard motor-driven pumps (microcompressors). Many options exist for driving a pump, including AC/DC electric motor, internal combustion engine, piezoelectric actuator, or even chemical- or biological-based actuators. Pump options include diaphragm, piston, screw, vane, and centrifugal pumps and many others. Onboard energy sources include gasoline or other

hydrocarbons and many types of battery. While a detailed analysis of these technologies is outside the scope of this article and can be found in the literature,<sup>24–28</sup> a general discussion of the suitability for soft robotics is in order. Internal combustion engines are generally large and loud and emit hot toxic gasses, restricting them to large-scale outdoor operations.<sup>29,30</sup>

AC electric motors are also generally too large for mobile soft robotic needs. Unlike most air compressor technologies, diaphragm pumps are commercially available in form factors sufficiently small for soft robotic applications. Diaphragm pumps oscillate a membrane, displacing air inside a chamber with check valves at the inlet and outlet to generate airflow and pressure differential. While very small piezoelectric diaphragm pumps are available,<sup>31</sup> they generally provide insufficient flow rate and pressure for soft robots (MuRata specifies 0.8 SLM, 1.5 kPa). Several DC motor-based diaphragm microcompressors are commercially available and have been used in previous soft robots,<sup>32,33</sup> and so we focus our investigation on these devices. Many battery chemistries are available, but the soft robotics community is converging on lithium polymer batteries utilizing the benefits of high energy and power densities and availability in many form factors and capacities.<sup>2,12,32</sup>

Virtually all robots require electrical power for control regardless of the type of primary actuation, and so a battery-based microcompressor does not require a second energy source. For increased pressure or flow rate, multiple microcompressors can be connected in series or parallel (Fig. 2), adding to their versatility. The use of microcompressors allows the possibility of regeneration (Fig. 2), routing exhaust air back into the pumping system rather than venting to atmosphere. In some applications, it may be possible to re-charge batteries using ambient solar energy or other energy-harvesting

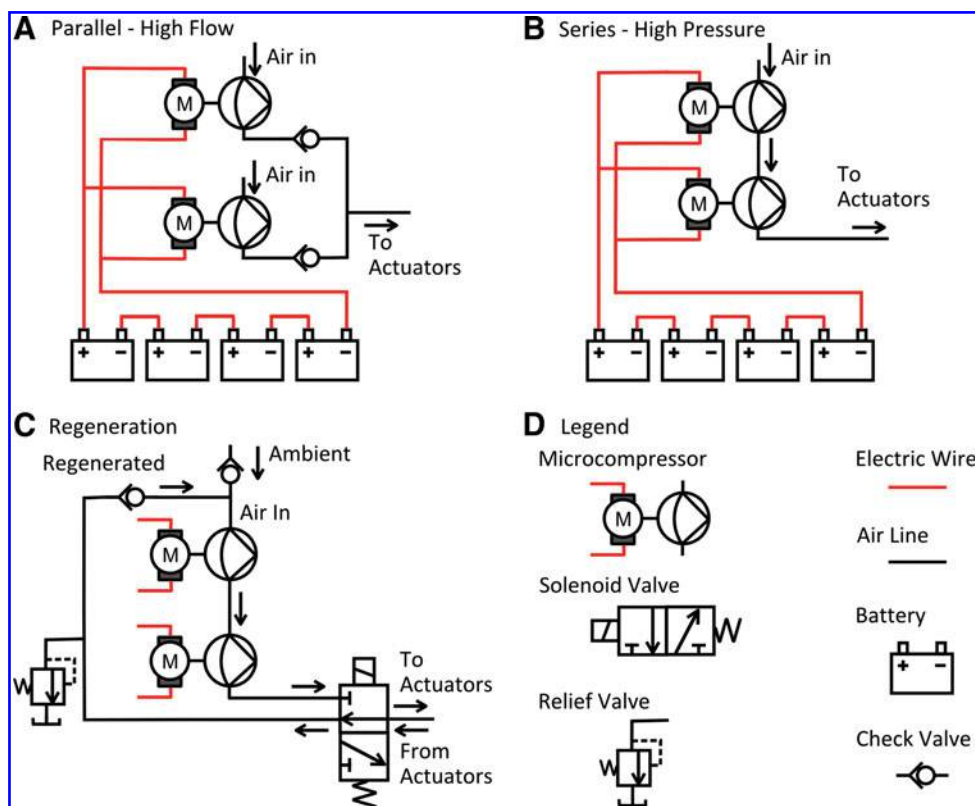


**FIG. 2.** (A) Microcompressors configured in parallel to increase volumetric flow rate. (B) Configured in series to increase final pressure. (C) Using actuator exhaust as pump input. (D) Legend. Color images available online at [www.liebertpub.com/soro](http://www.liebertpub.com/soro)

methods. While microcompressors add considerable static mass, this mass does not change when battery capacity is increased, beneficial in to scaling up. Battery-based microcompressors have the drawbacks of emitting considerable noise and having maximum pressures and flow rates orders of magnitude below those achievable with other options. Extensive hardware and numerous moving parts are required, contributing to overall static mass. To compensate for low maximum flow rate, compressed air can be stored in a plenum (a reservoir to store pressurized working gas) and released in short bursts. However, this configuration increases the fuel system size, requires pump-up time prior to device operation, and is only useful at low duty cycles (if gas is consumed continuously, it has no chance to accumulate in a plenum).

### Methods

**Microcompressor.** At the scale of current soft robotic applications, diaphragm pumps are the preferred microcompressor option, with the Parker Hargraves line used in several previous soft robotic applications.<sup>32,33</sup> For that reason, we selected the largest (BTC-IIs) and smallest (CTS) pumps from that line for evaluation. We tested the large and small microcompressors in three configurations (single, two in series, and two in parallel)—six configurations in total, in conditions consistent with previous soft robotics work.<sup>32,33</sup> We fed the compressed air from each configuration through a test fixture to monitor cylinder conditions (Fig. 3, right). We found the maximum pressure for all configurations by briefly blocking the flow directly after the upstream pressure gauge (item 2 in Fig. 3) and recording pressure. We found the maximum flow rate by connecting the compressed air (item 1 in Fig. 3) just before the thermocouple (item 6 in Fig. 3), eliminating the other components (items 2–5 in Fig. 3) to minimize flow resistance. Similar to blocked torque and unloaded RPM specifications for motors, these values provide a useful framework

for comparing pumps and configurations. We calculate useable work by dividing compression energy in the resulting gas (from the ideal gas law) by the battery energy output (from voltage and current data). While efficiency and flow data would change if microcompressors were operated at high or low voltage, it is anticipated that users will run microcompressors at or near their rated values. Users who require voltage very different from pump ratings should conduct their own tests or select a microcompressor rated for their application.

**Batteries.** We conducted all experiments using four-cell (14.8 V nominal) lithium polymer batteries with capacity as indicated. We fully charged all batteries prior to each experiment and terminated experiments when voltage dropped below 13.5 V to avoid damaging the batteries. Commercial batteries are typically rated in amp hours (Ah), which can be converted to nominal energy content (Wh, kJ) knowing the number of cells (3.7 V each). We tested each configuration using 800 mAh batteries for every pressure set point, and ran a second test at the maximum efficiency point. Additionally, we tested large microcompressors using 1250, 3200, and 4000 mAh batteries and tested small microcompressors using 120 and 450 mAh batteries, all at the pumps' pressures of maximum efficiency. At high consumption rates, the available energy in lithium polymer batteries drops. We designed all experiments so that energy was consumed at less than 4 C (1/4 h to consume the batteries' energy); thus, the rate of use had little effect on available energy.

**Test fixture.** We designed a test fixture to provide an impedance range similar to those found in current soft robots<sup>1,32</sup> while monitoring flow rate and upstream and downstream, temperature and pressure (Fig. 3). We verified that downstream air was at ambient temperature and pressure, confirming our constant-temperature assumption.

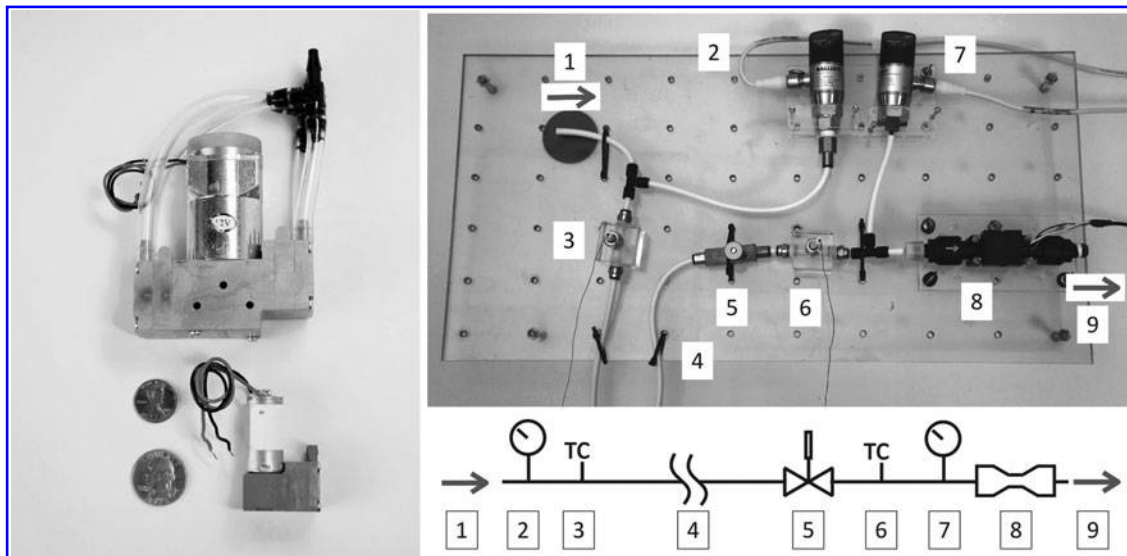


**FIG. 3.** (Left) Parker Hargraves microcompressors (large: BTC-IIs, specified as 12 V, 11 L/min 28 psig max; small: CTS, specified as 12 V, 1.8 L/min, 21 psig max). (Right) Photograph and schematic of test setup. 1. Pressurized air in from pneumatics source. 2. Upstream pressure gauge (Balluff BSP-B). 3. Upstream K-type thermocouple. 4. Twenty meters of tubing, 3 mm inner diameter, as load. 5. Needle valve to adjust load. 6. Downstream K-type thermocouple. 7. Downstream pressure gauge (Balluff BSP-B). 8. Hot wire anemometer flow meter (Honeywell AWM5000). 9. Ambient air out.

We tested all pump configurations from minimum pressure to near maximum pressure, setting pressure in increments of 50 kPa with the needle valve (Item 5 in Fig. 3). We used voltage, current, and time data to calculate battery energy output and we used flow rate, and time data to calculate total flow. We calculated air compression energy using downstream pressure, upstream pressure, and the ideal gas law.

**Results**

**Microcompressor.** Microcompressors exhibited high overall flow capacities but low maximum flow rates and pressures. Series configurations showed maximum efficiencies at higher pressures, while microcompressors in parallel produced higher flow rates (Table 1). Between successive tests and at various battery capacities, variability was less than 10% in flow rate and 1.6% in efficiency. Figure 4A shows battery and air compression energy data. Figure 4B shows characteristics needed to configure a microcompressor-based fuel system. Figure 4C shows mass data for all tested configurations and battery capacities. These plots are used to configure a microcompressor-based pneumatic system as described below. Key properties are given in Table 1, in which values are taken at the pressure of maximum efficiency. Energy density and flow capacity were calculated with 800 mAh batteries. These values would be higher for larger batteries, because gross fuel would be a larger portion of fuel system mass. The reverse would be true for smaller batteries.

**Example: soft pneumatic system configuration.** Knowing the soft robot’s requirements, we select a configuration of microcompressor (Fig. 4B) that will provide the required flow rate at the desired operating pressure. We find the required battery capacity (in Ah) by dividing the desired run time (min) by the normalized run time (min/Ah) (Fig. 4B). Based on the selected compressors and batteries, we find the system mass (Fig. 4C). For example, if a flow rate of 15 SLM at 100 kPa is required, we select the large parallel microcompressor configuration based on the flow rate versus pressure curve (Fig. 4B). If only three SLM had been required, the small parallel or any large microcompressor configuration could have been selected. Run time is 20 min/Ah (Fig. 4B). If the device will be running at 100% duty cycle, and 60 min of actuation is desired, a battery of 3000 mAh or larger capacity should be selected. Static mass for two parallel microcompressors is 667.4 g (Fig. 4C), and the gross fuel mass of a 3200 mAh battery is 325.9 g, for a fuel system mass of 993.3 g.

**Compressed Fluid**

**Concept**

**Thermodynamics.** Compressed fluid cylinders can provide pneumatic energy at high pressure and flow rate and can be stored for extended periods prior to opening (e.g., life preservers, portable tire inflator, and inflatable boats), all in a relatively small package. The most commonly used fluids are air compressed to 20 or 30 MPa and CO<sub>2</sub> stored as a liquid at 5.6 MPa. As gas is regulated to a working pressure and allowed to flow from its storage container, temperature drops (this varies with conditions, but -40°C was commonly seen

TABLE 1. KEY VALUES: MICROCOMPRESSOR

	Max. pressure (no flow) (kPa)	Max. flow rate (min. pressure) (SLM)	Pressure at peak efficiency pres. effic. (kPa)	Flow rate (SLM)	Total flow (L)	Battery life <sup>a</sup> (min/Ah)	Net energy <sup>b</sup> (kJ)	Mass		Energy density		Flow capacity	
								Static (g)	Fuel sys. (g)	Gross fuel (J/g)	Fuel sys. (J/g)	Gross fuel (L/g)	Fuel sys. (L/g)
1 Small	200	2.6	100	1.70	178.9	131.8	12.9	41.3	129.9	145.6	99.3	2.02	1.38
2 Small, parallel	210	5.9	100	3.51	211.4	76.1	13.6	82.6	171.2	152.9	79.2	2.39	1.23
2 Small, series	340	3.6	150	2.79	133.6	59.7	12.4	82.6	171.2	140.3	72.6	1.51	0.78
1 Large	260	14.1	150	5.71	158.2	34.9	14.2	333.7	422.3	160.0	33.6	1.79	0.37
2 Large, parallel	270	27.3	150	10.72	154.5	18.3	14.0	667.4	756.0	158.0	18.5	1.74	0.20
2 Large, series	550	13.2	150	9.67	125.6	16.5	11.2	667.4	756.0	126.6	14.8	1.42	0.17

Values for 800 mAh 4S batteries (88.6 g gross fuel mass). Adjust energy density values for larger or smaller batteries. Pressure is set for maximum efficiency for each configuration.

<sup>a</sup>Based on 100% duty cycle operation.

<sup>b</sup>From pressure measurements and the ideal gas law.

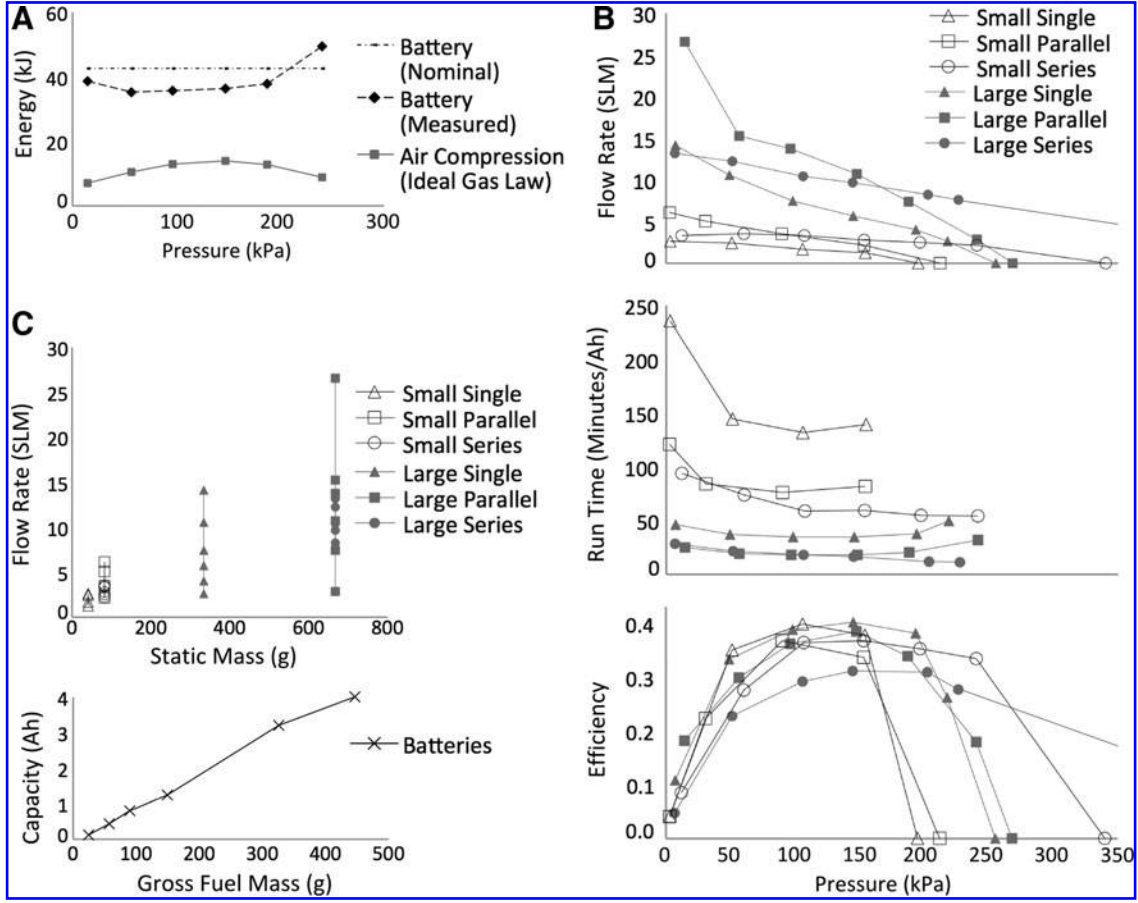


**FIG. 4.** Microcompressor flow characteristics. **(A)** Energy versus pressure. Large parallel microcompressors shown as an example. Nominal energy taken from the battery data sheet ( $2 \times 2$  S 800 mAh batteries). Battery-measured energy was calculated from recorded voltage and current data. Air compression energy was calculated from the ideal gas law,  $w = P \times V \times \ln(P_2/P_1)$ . **(B)** Normalized flow rate, run time, and efficiency versus gauge pressure for six-pump configurations. At minimum pressure, there was little compression (small  $P_2/P_1$ ); at maximum pressure, there was little total flow (small  $V$ ). Thus, useful pneumatic energy was low at both extremes, yielding low efficiency. **(C)** Flow rate versus static mass and battery capacity versus gross fuel mass for all microcompressors and batteries tested.

during testing), allowing heat transfer from the environment into the expanding gas. In high-speed applications (e.g., paintball, the Boston Dynamics Sand Flea<sup>34</sup>), little energy can be transferred to the working fluid during actuation, yielding near-adiabatic conditions. Conversely, serving as an upper limit, capacity tests were performed in isothermal conditions to allow comparison between configurations. The designer can anticipate that at low flow rates (previous soft robots have operated below 10 SLM at 100 kPa<sup>1,12</sup>) conditions will be polytropic but most likely nearer to isothermal than to adiabatic.

**Pressure vessel: gross energy density.** Because a pressure vessel requires considerable mechanical integrity, cylinder mass is a substantial portion of the gross fuel mass. Beginning with air, we use the ideal gas law to calculate the total energy stored per unit mass:

$$PV = nRT \quad (1)$$

where  $P$  is pressure,  $V$  is volume,  $n$  is number of molecules of gas,  $R$  is the universal gas constant, and  $T$  is temperature.

Calculating energy as the integral of the pressure with the change in volume (assuming isothermal conditions) yields

$$W_{1-2} = P_1 V_1 \ln\left(\frac{P_2}{P_1}\right) \quad (2)$$

where  $W$  is the work,  $P_1$  is initial pressure,  $V_1$  is initial volume, and  $P_2$  is final pressure. Net fuel energy densities are reported in Table 2. To calculate the gross fuel energy density, we determine the theoretical geometry and mass of a containment vessel. We begin with aluminum (AL 6061-T6, yield stress of 276 MPa, density of 2.7 g/cc, factor of safety of two<sup>35</sup>). Using thick wall pressure vessel theory, we obtain

$$\sigma = p_i \frac{r_o^2 + r_i^2}{r_o^2 - r_i^2} \quad (3)$$

Solving for  $r_o$ , Equation 3 becomes

$$r_o = \sqrt{\frac{\sigma + p_i}{\sigma - p_i}} r_i \quad (4)$$

TABLE 2. THEORETICAL ENERGY DENSITIES AND FLOW CAPACITIES FOR A CYLINDER OF COMPRESSED FLUID

	<i>Vessel mass per gram of fuel (g/g)</i>	<i>Energy density</i>		<i>Flow capacity @ stp</i>	
		<i>Net fuel (J/g)</i>	<i>Gross fuel (J/g)</i>	<i>Net fuel (L/g)</i>	<i>Gross fuel (L/g)</i>
Air 20 MPa, Al tank	6.16	440.1	61.5	0.774	0.108
Air 30 MPa, Al tank	7.03	473.7	59.0	0.774	0.096
CO <sub>2</sub> 5.6 MPa, steel tank	1.19	219.9	151.2	0.509	0.351

yielding the gross fuel energy densities in Table 2. Air at 30 MPa has a net fuel energy density only 7.7% higher than air at 20 MPa (due to the natural log-term in Eq. 2). Because of the considerable additional vessel weight required to contain air at 30 MPa, gross fuel energy density actually decreases.

Considering liquid CO<sub>2</sub> at 5.6 MPa using a density of  $7.70 \times 10^5$  g/m<sup>3</sup>, we use the van der Waals formula

$$nRT = \ln \left[ \frac{V_2 - nb}{V_1 - nb} \right] - an^2 \left[ \frac{1}{V_1} - \frac{1}{V_2} \right] \quad (5)$$

where  $a = 3.592$  (L<sup>2</sup>·atm)/mol<sup>2</sup> and  $b = 0.04267$  L/mol, to calculate work done by a nonideal gas as the liquid vaporizes and expands to 1 atm. For cost and manufacturing reasons, small quantities of CO<sub>2</sub> are often sold in single-use steel cylinders. Repeating pressure vessel calculations for steel (alloy SA537 class 2 steel, with a density of 7.85 g/cc, a yield strength of 315 MPa, and safety factor of two) yields the gross fuel energy density in Table 2. Again, the fuel with lower net fuel energy density has a higher gross fuel energy density due to reduced containment vessel mass. Here, vessel mass is lower because of lower stresses (lower  $P_i$ ) and because the denser liquid CO<sub>2</sub> occupies a smaller volume (smaller  $r_i$ ).

Commercial vessels include considerable additional material for mechanical ports, safety hardware, and for manufacturability, and so real cylinders are considerably heavier than theory would suggest. To contain 30 MPa air, aluminum cylinders would be extremely heavy; thus, commercial cylinders are typically complex designs including a thin aluminum shell surrounded by a custom-designed layup of aramid and polymer composite. A detailed analysis of composite layup design is outside the scope of this article, and so cylinder masses are given for actual tanks (Table 3), but no theoretical values are given (Table 2).

Applications requiring sustained high flow rates (e.g., paint ball) tend to use compressed air cylinders over CO<sub>2</sub>. Though liquid-phase storage allows for compact design, rapid vaporization expels very cold gas or even liquid ( $-40^\circ\text{C}$  was seen regularly during our experiments) that can cause clogging of the lines or regulator seizing, leading to short-term failure or permanent system damage.

Energy density versus effective energy density. Energy density values for compressed air and CO<sub>2</sub> can be misleading. Work is a function of the natural log of the pressure ratio (Eq. 2 as shown in Fig. 5). Thus, air stored at 30 MPa has an energy density of 473.7 J/g, but if regulated to 500 kPa prior to use,

TABLE 3. KEY VALUES: COMPRESSED FLUID CYLINDERS

	<i>Mass</i>				<i>Max. flow rate<sup>a</sup> (SLM)</i>	<i>Total flow (std. liter)</i>	<i>Energy<sup>b</sup></i>		<i>Energy dens.<sup>c</sup></i>		<i>Flow capacity</i>	
	<i>Net fuel (g)</i>	<i>Gross fuel (g)</i>	<i>Static (g)</i>	<i>Fuel system (g)</i>			<i>Theory (kJ)</i>	<i>0.5 MPa (kJ)</i>	<i>Net fuel (J/g)</i>	<i>Fuel system (J/g)</i>	<i>Net fuel (L/g)</i>	<i>Fuel system (L/g)</i>
CO <sub>2</sub> 8 g	7.8	33.6	16.3	49.9	18	4.1	1.70	0.66	219.9	34.2	0.51	0.082
CO <sub>2</sub> 12 g	11.7	41.9	16.3	58.2	18	6.2	2.56	0.99	219.9	44.1	0.51	0.106
CO <sub>2</sub> 16 g	17.4	57.7	53.5	111	18	8.6	3.82	1.48	219.9	34.4	0.51	0.077
CO <sub>2</sub> 45 g	46.9	185	227	412	127	25.1	10.3	4.00	219.9	30.4	0.51	0.074
CO <sub>2</sub> 74 g	70.7	298	227	524	127	38.4	15.5	6.01	219.9	34.4	0.51	0.085
CO <sub>2</sub> 94 g	86.1	435	227	662	127	46.8	18.9	7.33	219.9	32.1	0.51	0.08
CO <sub>2</sub> 20 oz	416	1281	291	1573	300	212.1	91.4	35.5	219.9	58.1	0.51	0.135
Air 13 in <sup>3</sup>	56.0	513	395	909	350	43.1	24.6	12.1	440.1	27.1	0.77	0.047
20 MPa												
Air 48 in <sup>3</sup>	196	1579	395	1975	350	151.1	86.3	42.5	440.1	43.7	0.77	0.077
20 MPa												
Air 68 in <sup>3</sup>	333	1490	395	1885	650	256.3	157.6	49.5	473.7	83.6	0.77	0.136
30 MPa												

Commercial CO<sub>2</sub> cylinders are described by nominal net fuel mass. Air cylinders are described by internal volume and maximum allowable pressure. In our tests, 20 oz CO<sub>2</sub> and all air cylinders are refillable. All other CO<sub>2</sub> cylinders are single use. Fitting and plumbing sizes increase with cylinder size, yielding increased static mass and max flow rate in larger units.

<sup>a</sup>Highest observed for canister size and corresponding hardware.

<sup>b</sup>Theoretical at full cylinder pressure and regulated to 0.5 MPa working pressure.

<sup>c</sup>Contained in gas at stored pressure. Not reduced working pressure.

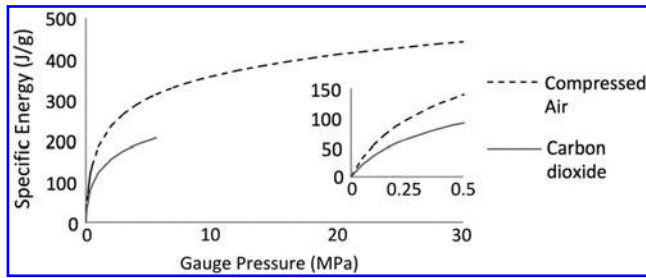


**FIG. 5.** Stored energy versus working energy. Main graph: overall. Inset: detail, 0.0–0.5 MPa. Most soft robots operate below 0.5 MPa. For the same mass of working fluid, reducing the working pressure reduces the effective energy density.

energy density drops to 138.6 J/g, for an efficiency of 31.4%. An amount of 20 MPa air and liquid CO<sub>2</sub> regulated to 500 kPa energy drops to 138.6 and 91.2 J/g, respectively, for efficiencies of 38.8% and 49.2%, respectively. Regulated to lower working pressures, an even greater portion of energy will go unused.

Compressed fluid cylinders have the advantages of high pressure and flow rate and operate more quietly than micro-compressors. With phase change and rapid expansion, CO<sub>2</sub> becomes very cold and can be used as a heat sink or to thermally camouflage a robot in cold environments. Because no compressor is required, static mass can be low. When using compressed air, there are no harmful chemical by-products, which is especially important in wearable devices.<sup>2,17</sup> Disadvantages include a system flow capacity (Table 2) an order of magnitude lower than that of micro-compressors (Table 1). Most of the stored energy is not used in low-pressure applications. To contain the pressurized fluid, a hard/heavy containment vessel is required, reducing gross fuel energy density. If using CO<sub>2</sub>, one must exercise caution regarding thermal management when designing the gas delivery system.

#### Method

**Compressed fluid.** We tested a refillable CO<sub>2</sub> cylinder, single-use CO<sub>2</sub> cylinders, and refillable compressed air cylinders using the flow test system described in the Micro-compressor section (Fig. 3). During these tests, we immersed the 20 m of tubing in a bath of water at ambient temperature to ensure isothermal conditions. Because the flow meter was

calibrated for air, we used heat capacity conversion factors suggested by the manufacturer for CO<sub>2</sub>. To approximate quasi-static, isothermal conditions, we set the upstream pressure to 100 kPa using an electronic regulator (ER1 Wilkerson), resulting in a flow rate of less than 10 SLM for air and less than 5 SLM for CO<sub>2</sub>. This served as a virtual load with impedance similar to that seen in previous soft robots.<sup>1,12</sup> To verify assumptions of ambient conditions, we monitored downstream temperature and pressure (Fig. 3). We tested the maximum flow rate for each cylinder by measuring the change in mass after allowing the cylinder to flow freely by opening a ball valve for 3 s and repeated until each tank was empty. We monitored each tank surface temperature with an infrared thermometer. All cylinder sizes were tested twice.

#### Results

**Compressed fluid.** Total flow of air and CO<sub>2</sub> cylinders was very close to theory (Fig. 6). Maximum flow rate for air and CO<sub>2</sub> is given in Table 3 with other key values for compressed fluid cylinders. In all single-use cylinders, flow rate was limited by CO<sub>2</sub> freezing in the lines. Maximum flow is the highest rate we achieved with standard hardware and serves as a general guideline for design. Custom configurations could be designed to increase these values while restrictive plumbing would reduce them. Because reusable tanks were filled manually at a retail outlet<sup>36</sup> by pressure rather than mass, variability between successive fills is high but fuel content was determined from change in tank mass.

#### Direct Chemical Reaction

In the previous sections, we discussed microcompressors that rely on lithium ions inside a battery, and we discussed compressed fluid cylinders that use the expansion of a pressurized gas and phase change. Neither of these processes uses chemical reaction to directly generate the working pneumatic pressure. We identify three options for direct chemical reaction: monopropellant decomposition, hypergolic reaction, and combustion. Monopropellant decomposition consists of a chemical breaking down exothermically in the presence of a catalyst, not requiring a separate oxidizer. Hypergolic reactions consist of two chemicals spontaneously igniting when in contact with one another. Combustion consists of a fuel and oxidizer reacting in the presence of a spark/flame. Hypergolic propellants tend to be highly toxic, and thus they will not be covered. In some reactions pneumatic pressure is

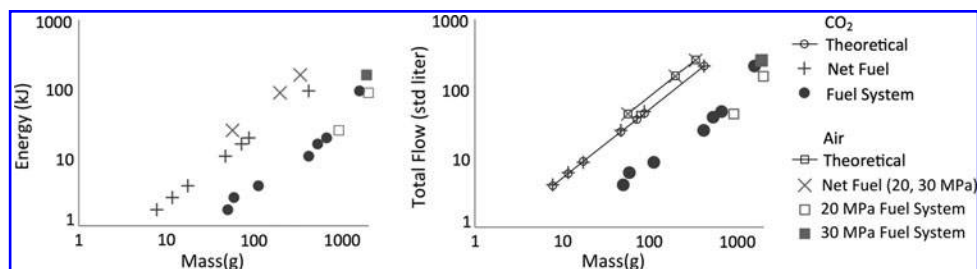


**FIG. 6.** (Left) Energy density. (Right) Total flow for CO<sub>2</sub> and air cylinders. Measured flow was within 3% of theoretical for all cylinders. Gross fuel values omitted for clarity. Air cylinders of 30 MPa were fiberglass composites and thus had lower mass than 20 MPa aluminum cylinders. High-pressure air cylinders were not commercially available in very small volumes; thus, all cylinders below 900 g fuel system mass were CO<sub>2</sub>.

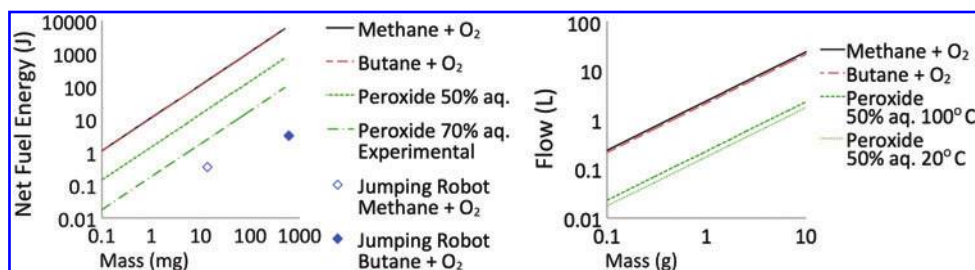
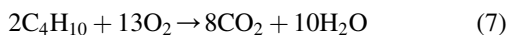
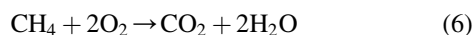


**FIG. 7.** (Left) Net fuel energy versus mass, combustion, and decomposition (theoretical). Experimental hydrogen peroxide 70% aq. in a rigid fuel system, lifting a mass,<sup>39</sup> and jumping robots.<sup>6,32</sup> (Right) Theoretical flow versus mass. Color images available online at [www.liebertpub.com/soro](http://www.liebertpub.com/soro)

produced partially by the increase in mols of gas, but the primary source of gas pressure is from the heat of reaction. As the resultant gas cools, this pressure would be lost, and thus these reactions are generally performed as needed, often at the point of use. There have been investigations into chemical reactions for autonomous robots,<sup>37–40</sup> prostheses,<sup>41</sup> and even soft mobile robotics<sup>6,12,32,42</sup> at the research level with each system custom designed for its particular application. While many fuels are available, we have chosen to evaluate methane and butane combustion and hydrogen peroxide decomposition because they appear to be the most viable and are supported by published data in relevant applications.

#### Explosive combustion

The combustion of methane and butane follow the stoichiometric equations:



releasing 890 kJ/mol and 2.88 MJ/mol of heat, respectively, and commonly occur quickly enough to be considered explosive. Methane and butane combustion have the advantage of being the highest energy densities and highest speed reactions discussed in this article, making them extremely useful for high-power applications such as jumping. Combustion has disadvantages of being loud and resulting in very high local temperatures. Combustion requires onboard fuel and oxygen sources (or use of ambient air), ignition source, valves and control hardware for precise stoichiometry, and

mechanical mixing followed by sparking. All of these requirements dictate considerable development effort and system integration. Byproducts of combustion include steam and heat, which can be hazardous. Due to the very rapid reaction, combustion in soft systems is difficult to model; in addition to nonlinear deformation, one must model transient events. Due to limitations in the experimental mechanical design, previous work in methane-based jumping yielded efficiency of only  $\sim 0.7\%$ <sup>6</sup> for a useable energy of only  $\sim 350$  mJ; however, this energy was released at a rate of 35 W, causing the device to jump 30 times its height. Given the high energy densities and reaction rates found in hydrocarbons, combustion remains an exciting area for development as a pneumatic energy source.

#### Peroxide monopropellant

The decomposition of hydrogen peroxide follows the formula:



releasing 98.2 kJ/mol in heat. Relying on only a small amount of catalyst, hydrogen peroxide decomposition has the advantage of not requiring exact chemical ratios or an ignition source to initiate the reaction. While not commercially available, a peroxide fuel system would require minimal static mass, making it a promising option for small-scale pneumatic systems and for a fully soft or primarily soft pneumatic fuel source. Concentrated peroxide ( $>70\%$ ) contains enough energy to vaporize all byproducts, increasing chances of explosion, and so less concentrated aqueous mixtures are often used, reducing energy density. While

TABLE 4. KEY VALUES: DIRECT CHEMICAL REACTION

	Theoretical net fuel		Fuel mass		Experimental energy density				
	Energy density (kJ/g)	Flow capacity (L/g)	Net fuel (g)	Fuel system (g)	Energy measured (J)	Net fuel (J/g)	Fuel system (J/g)	Efficiency (%)	Fuel system flow capacity (L/g)
Methane + O <sub>2</sub>	11.1	2.38	0.04	n.a.	0.35	8.75	n.a.	0.7% <sup>5</sup>	n.a.
Butane + O <sub>2</sub>	10.8	2.15	2.75	62.7	3 J/jump	54	2.37	0.5% <sup>28</sup>	0.094
Hydrogen peroxide 50%	1.44	0.18–0.23	76 <sup>8</sup>	357	n.a.	n.a.	10–28 <sup>a</sup>	3.3–9%, 45% <sup>b</sup>	0.04–0.05 <sup>a</sup>

Combustion includes fuel and oxygen mass and assumes reaction products at 500°C. For decomposition, assumes O<sub>2</sub> at 20°C and 100°C. Methane is supplied via tether, and thus no system-level values are available.<sup>6</sup> Butane reaction was oxygen limited, and so assume that oxygen was replenished until fuel was exhausted.

<sup>a</sup>Net fuel and fuel system masses from Onal *et al.*<sup>12</sup> multiplying theoretical energy density by 3.3% and 9% efficiency from Fite and Goldfarb.<sup>39</sup>

<sup>b</sup>Experiments with 70% by mass hydrogen peroxide.<sup>37–39</sup> Note, 45% efficiency based on effective energy density of 400 kJ/kg versus total energy density of 2000 kJ/kg for 70% hydrogen peroxide, raising efficiency from 9% to 45%.

TABLE 5. KEY VALUES: FUEL SYSTEM-LEVEL SUMMARY

	Fuel system mass as evaluated (g)	Maximum pressure (MPa)	Maximum flow rate (SLM)	Fuel system energy density (J/g)	Efficiency as evaluated %	Fuel system flow capacity (L/g)
Microcompressor small	130–171	0.2–0.34	1.7–3.5	72.6–99.3	36.7–39.9%	0.78–1.38
Microcompressor large	422–756	0.26–0.55	5.7–10.7	14.8–33.6	31.2–40.3%	0.17–0.37
Liquid CO <sub>2</sub> small	49.9–662	5.6	18–127	30.4–44.1	< 49% <sup>a</sup>	0.074–0.11
Liquid CO <sub>2</sub> (refillable)	1573	5.6	300	58.1	< 49% <sup>a</sup>	0.14
Air cylinder (refillable)	909–1975	20 and 30	350–650	27.1–83.6	< 39% <sup>a</sup>	0.05–0.14
Butane combustion <sup>32</sup>	62.7	n.a.	n.a.	2.37	0.5%	0.094
Hydrogen peroxide decomposition	357 <sup>12</sup>	0.0507 <sup>12</sup>	n.a.	10–28 <sup>b</sup>	3.3–9%, 45% <sup>37–40</sup>	0.04–0.05 <sup>12,c</sup>

Microcompressor values are for 800mAh batteries at pressure of maximum efficiency. Air and CO<sub>2</sub> are for stored pressure, not reduced working pressure. Butane and hydrogen peroxide values are from the literature based on custom architecture and may not represent future designs. Methane was supplied via tether, and so fuel system mass not applicable.<sup>6</sup> No maximum pressure and rate values are available for butane.<sup>32</sup>

<sup>a</sup>Assumes working pressures of 0.5 MPa and isothermal conditions. Polytropic systems at lower operating pressures will have lower values.

<sup>b</sup>Based on mass of pneumatic battery<sup>12</sup> and efficiency of 3.3–9% of 1.44 kJ/g net fuel.<sup>37–40</sup>

<sup>c</sup>Range assumes that all reaction products are liquid between 20°C and 100°C.

resulting water and oxygen are not harmful, the heat can be a hazard. Goldfarb *et al.* showed useful work with 70% peroxide of 180 J/g for an efficiency of 9.0% using a rigid pressure chamber-based system.<sup>38</sup> A hydrogen peroxide-based pneumatic battery has been developed to propel a soft robot,<sup>12</sup> focusing on the design of this novel system rather than quantifying energetics.

#### Key values: direct chemical reaction

Stoichiometric equations give the total energy released, but the state (pressure, temperature, and phase) of the products depends on many factors, including environment and system design. Shepherd *et al.* found that reaction byproducts exceeded 500°C<sup>6</sup>; thus, we use 500°C for calculations. For

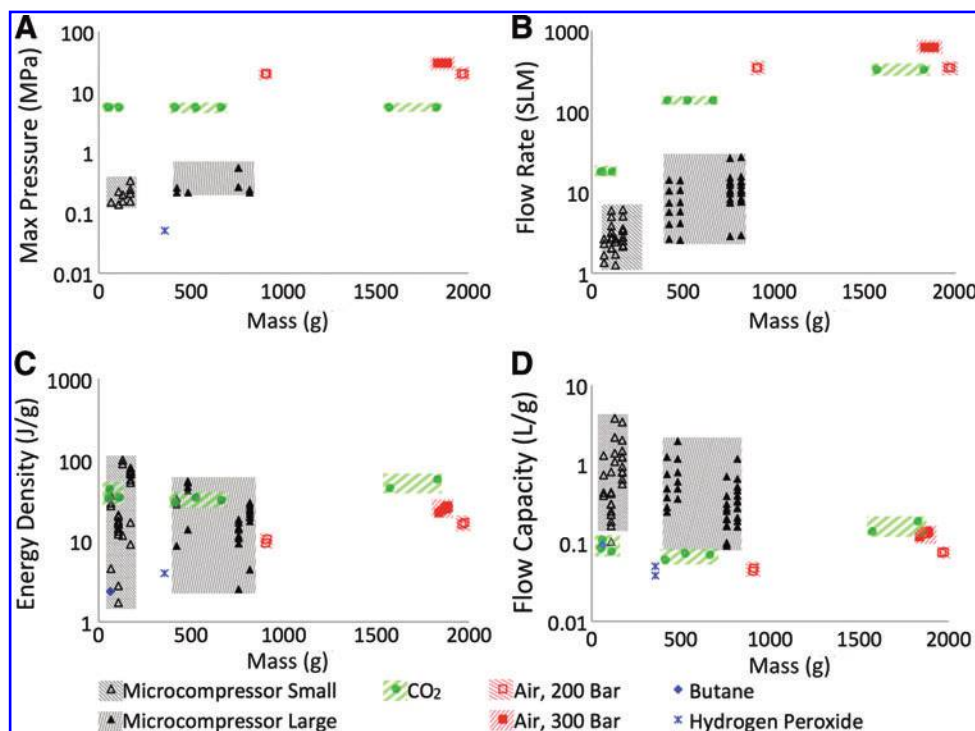


**FIG. 8.** Key values as tested. Ordinate axes are log scale. Mass values are fuel system mass. All microcompressor pressures and battery sizes are shown, so ranges and weights vary more widely than in Table 5. Mass variation in air and CO<sub>2</sub> cylinders are due to variation during filling. Methane was supplied via tether, so fuel system mass was not applicable.<sup>6</sup> (A) Maximum pressure. Microcompressor values are experimental. Air and CO<sub>2</sub> are maximum cylinder pressure. Hydrogen peroxide pressure is from published experiments,<sup>12</sup> but alternative system design could yield higher pressures. (B) Maximum measured flow rate. (C) Fuel system energy density. Microcompressor values are from experiments. Cylinder values are based on a 0.5 MPa working pressure and isothermal assumption. Butane and hydrogen peroxide are from Table 5. (D) Flow capacity. Microcompressor and cylinder values are from experiments. Butane and hydrogen peroxide values are from Table 5. Color images available online at [www.liebertpub.com/soro](http://www.liebertpub.com/soro)

decomposition, we consider aqueous hydrogen peroxide (50 wt%), yielding liquid water and oxygen gas between 20°C and 100°C. Net energy density and flow capacity as well as published values for experimental work (Fig. 7) are given in Table 4.

## Discussion

In designing a pneumatic energy system, it is tempting to simply select the technology with the highest energy density or flow capacity; however, it is important to select a technology to match the application. If key parameters such as flow rate and maximum pressure are not aligned, either the source will struggle to meet the requirements, or overpressure gas will burst forth too quickly, wasting energy and making control difficult. System scale may drive technology decisions as small systems are dominated by static mass where larger scale systems are dominated by gross fuel energy density. It would be undesirable to attach a 50 g micro-compressor to a 10 g soft robot, regardless of battery energy density; however, at human scale, a static mass of several kilograms is realistic. Technology readiness level must be considered for combustion and monopropellant decomposition in which custom systems must be designed for each application. Factors such as noise, high local temperatures, and toxic byproducts should be considered. Table 5 gives key system-level parameters for selecting a pneumatic energy source. Figure 8 gives key values for systems as tested. Note that system-level values are considerably different from net fuel values discussed earlier.

At low pressure and flow rate, microcompressors are often the best choice for soft robotic applications because they offer the highest flow capacity available in a commercial package. If higher pressure or flow is needed, CO<sub>2</sub> cylinders should be considered. If the application will require continuous high flow rates, high-pressure air cylinders will avoid seize or freezing due to the endothermic expansion of CO<sub>2</sub>. If even faster actuation is needed (such as in very high speed jumping), combustion may be considered but will require considerable development effort. For very-small-scale applications, monopropellant decomposition may provide the lowest static mass but will also require considerable development. If an application will require vastly different types of motion (for example slow crawling followed by jumping), a hybrid system should be considered, in which different types of actuation are achieved with different pneumatic technologies.<sup>32</sup> By characterizing pneumatic energy systems, we have provided a system-level framework to support the design of untethered pneumatic soft robots and soft wearable. In the future, it would be beneficial to characterize direct chemical reactions in soft robots at the system level. For this effort, it will be necessary to develop stand-alone monopropellant and combustion-based pneumatic power supplies, and to quantify the anticipated fuel capacity and flow capabilities of the system.

## Acknowledgments

This work was partially supported by The Defense Advanced Research Projects Agency (award # W911NF-11-1-0094), the National Science Foundation (award # DMR-0820484), and the Wyss Institute for Biologically Inspired Engineering. Nicholas W. Bartlett of the Harvard School of

Engineering and Applied Sciences contributed to the preparation of this article.

## Disclaimer

Any opinions, findings, conclusions, or recommendations expressed in this article are those of the authors and do not necessarily reflect the views of the National Science Foundation.

## Author Disclosure Statement

No competing or financial interests exist.

## References

1. Shepherd RF, Ilievski F, Choi W, Morin SA, Stokes AA, Mazzeo AD, Chen X, Wang M, Whitesides GM. Multigait soft robot. *Proc Natl Acad Sc USA* 2011;108:20400–20403.
2. Park Y-L, Chen B, Perez-Arancibia N, Young D, Stirling L, Wood R, Goldfield E, Nagpal R. Design and control of a bio-inspired soft wearable robotic device for ankle-foot rehabilitation. *Bioinsp Biomimet* 2014;9.1:016007.
3. Majidi C. Soft robotics: a perspective current trends and prospects for the future. *Soft Robot* 2013;1:5–11.
4. Kim S, Laschi C, Trimmer B. Soft robotics: a bioinspired evolution in robotics. *Trends Biotechnol* 2013;31:287–294.
5. Park Y-L, Santos J, Galloway K, Goldfield E, Wood R. A Soft wearable robotic device for active knee motions using flat pneumatic artificial muscles. *Proceedings of the IEEE International Conference on Robotics and Automation, Hong Kong, 2014*, pp. 4805–4810.
6. Shepherd R, Stokes A, Freake J, Barber J, Snyder PW, Mazzeo ad, Cademartiri L, Morin SA, Whitesides GM. Using explosions to power a soft robot. *Angew Chem* 2013;125:2964–2968.
7. Illievski F, Mazzeo A, Shepherd R, Chen X, Whitesides GM. Soft robotics for chemists. *Angew Chem* 2011;123:1930–1935.
8. Lipson H. Challenges and opportunities for design, simulation, and fabrication of soft robots. *Soft Robot* 2013;1:21–27.
9. Cianchetti M, Ranzani T, Gerboni G, Nanayakkara T, Althoefer K, Dasgupta P, Menciassi A. Soft robotic technologies to address shortcomings in today's minimally invasive surgery: the STIFF-FLOP approach. *Soft Robot* 2014;1:122–131.
10. McMahan W, Chitrakaran V, Csencsits M, Dawson D, Walker I, Jones B, Pritts M, Dienno D, Grissom M, Rahn C. Field of trials and testing of the OctArm continuum manipulator. *IEEE International Conference on Robotics and Automation, Orlando, FL, 2006*, pp. 2336–2341.
11. Pauline M. SRL Spine Robot. 2013. <http://srl.org/machines/spine/index.php> (accessed Aug 26, 2014).
12. Onal C, Chen X, Whitesides G, Rus D. Soft mobile robots with on-board chemical pressure generation. *International Symposium on Robotics Research, 2011*.
13. iRobot Corporation. <http://spectrum.ieee.org/automaton/robotics/military-robots/irobot-developing-inflatable-robot-arms-inflatable-robots> (accessed Feb 13, 2014).
14. Deimel R, Brock O. A novel type of compliant, under-actuated robotic hand for dexterous grasping. *Robotics: Science and Systems, Berkeley, CA, 2014*, pp. 1687–1692.
15. Suzumori K, Endo S, Kanda T, Kato N, Suzuki H. A bending pneumatic rubber actuator realizing soft-bodied manta swimming robot. *IEEE International Conference on Robotics and Automation, Rome, Italy, 2007*, pp. 4975–4980.

16. Wehner M, Quinlivan B, Aubin P, Martinez-Villalpando E, Bauman M, Stirling L, Holt K, Wood RJ, Walsh C. Design and evaluation of a lightweight soft exosuit for gait assistance. IEEE International Conference on Robotics and Automation, Karlsruhe, Germany, 2013, pp. 3362–3369.
17. Wehner M, Park Y-L, Walsh C, Nagpal R, Wood RJ, Moore T, Goldfield E. Experimental characterization of components for active soft orthotics. Biomedical Robotics and Biomechatronics, Rome, Italy, 2012, pp. 1586–1592.
18. Tanaka T, Satoh Y, Kaneko S, Suzuki Y, Sakamoto N, Seki S. Smart suit: soft power suit with semi-active assist mechanism—prototype for supporting waist and knee joint. Proceedings of the 2008 International Conference on Control, Automation and Systems, Seoul, Korea, 2008, pp. 2002–2005.
19. Imamura Y, Tanaka T, Suzuki Y, Takizawa K, Yamanaka M. Motion-based-design of elastic material for passive assistive device using musculoskeletal model. J Robot Mechatron 2011;23.6:978–990.
20. Wehner M, Rempel D, Kazerooni H. Lower extremity exoskeleton reduces back forces in lifting. ASME 2009 Dynamic Systems and Control Conference, Los Angeles, CA, 2009, pp. 49–56.
21. Gaylord RH. Fluid actuated motor system and stroking device. U.S. Patent 2,844,126, July 22, 1958.
22. White F. Fluid Mechanics. New York: McGraw–Hill, 2010.
23. Parr A. Hydraulics and Pneumatics, 2nd ed. Burlington, MA: Butterworth-Heinemann, 1998.
24. Yeadon W, Yeadon A. Handbook of Small Electric Motors. New York: McGraw–Hill, 2001.
25. Dixon SL, Hall CA. Fluid Mechanics, Thermodynamics of Turbomachinery, 3rd ed. Burlington, MA: Pergamon Press, 1978.
26. Taylor C. The Internal Combustion Engine in Theory and Practice: Vol. 1, 2nd ed. Revised: Thermodynamics, Fluid Flow, Performance. Cambridge, MA: MIT Press, 1985.
27. Reddy T. Linden's Handbook of Batteries, 4th ed. New York: McGraw–Hill, 2010.
28. Epstein A. Millimeter-scale, micro-electro-mechanical systems gas turbine engines. J Eng Gas Turbines Power 2004;126.2:205–226.
29. Raibert M, Blankespoor K, Nelson G, Playter R. BigDog, the rough-terrain quadruped robot. Proceedings of the 17th World Congress of Automatic Control, 2008, pp. 10823–10825.
30. Zoss A, Kazerooni H, Chu A. Biomechanical design of the Berkeley Lower Extremity Exoskeleton (BLEEX). IEEE/ASME Trans Mechatron 2006;11:128–138.
31. MuRata. World's smallest low profile high pressure pump. www.murata-ps.com/emena/2012–05-22.html (accessed Jan 22, 2014).
32. Tolley M, Shepherd R, Karpelson M, Bartlett N, Galloway K, Wehner M, Nunes R, Whitesides G, Wood R. An untethered jumping soft robot. International Conference on Intelligent Robots and Systems (IROS), Chicago, IL, USA, 2014, pp. 561–566.
33. Mosadegh B, Polygerinos P, Keplinger C, Wennstedt S, Shepherd RF, Gupta U, Shim J, Bertoldi K, Walsh C, Whitesides G. Pneumatic networks for soft robotics that actuate rapidly. Adv Funct Mater 2014;24:2163–2170.
34. Ackerman E. Boston dynamics sand flea robot demonstrates astonishing jumping skills. IEEE Spectrum Robotics Blog, 2012.
35. Federal Register, 49CFR Part 107 p. 58462, Vol 63, no. 210, 1998.
36. www.bostonpaintballchelsea.com (accessed Jan 27, 2014).
37. Gogola M, Barth E, Goldfarb M. Monopropellant powered actuators for use in autonomous human-scaled robotics. IEEE International Conference on Robotics and Automation, Washington, DC, 2002, pp. 2357–2362.
38. Goldfarb M, Barth EJ, Gogola MA, Wehrmeyer JA. Design and energetic characterization of a liquid-propellant-powered actuator for self-powered robots. IEEE/ASME Trans Mechatron 2003;8:254–262.
39. Fite KB, Goldfarb M. Design and energetic characterization of a proportional-injector monopropellant-powered actuator. IEEE/ASME Trans Mechatron 2006;11:196–204.
40. McGee TG, Raade JW, Kazerooni H. Monopropellant-driven free piston hydraulic pump for mobile robotic systems. ASME J Dyn Syst Meas Contr 2004;126:75–81.
41. Sup F, Bohara A, Goldfarb M. Design and control of a powered transfemoral prosthesis. Int J Robot Res 2008; 27.2:263–273.
42. Messner W, Paik J, Shepherd R, Kim S, Trimmer B. Energy for biomimetic robots: challenges and solutions. Soft Robot 2014;1:106–109.

Address correspondence to:  
 Robert J. Wood, PhD  
 Microrobotics Lab  
 Harvard University  
 60 Oxford Street, #403  
 Cambridge, MA 02138

E-mail: rjwood@eecs.harvard.edu